A two-dimensional phase-field study on dendritic growth competition under convective conditions

V. Pavan Laxmipathy[a,b,*], Fei Wang[a], Michael Selzer[a,b], Britta Nestler[a,b]

[a] Institute of Applied Materials (IAM-CMS), Karlsruhe Institute of Technology (KIT), Strasse am Forum 7, 76131 Karlsruhe, Germany
[b] Institute of Digital Materials Science, Karlsruhe University of Applied Sciences, Moltkestr. 30, 76133 Karlsruhe, Germany

ARTICLE INFO

Keywords:
Dendritic growth competition
Melt convection
Isothermal solidification
Phase-field model

ABSTRACT

In the present work, the growth competition of columnar dendrites is investigated in the presence of melt convection. By using a multiphase-field model, the microstructural evolution of unidirectionally solidified dendrites with different crystal orientations is addressed in detail. Generally, for converging bicrystal grains, the dendritic growth competition follows a conventional overgrowth model, where a favorably oriented dendrite eliminates an unfavorably oriented dendrite at the grain boundary. However, in the presence of lateral melt flow in the liquid phase, we discover that the conventional overgrowth mechanism transforms into an unusual overgrowth mechanism as the melt velocity gradually increases. Recently observed in bi-crystal studies, the unfavorably oriented dendrites overgrow at the expense of the favorably oriented dendrites during an unusual overgrowth behavior. From our simulations we elucidate that the presence of an additional convective transport in the liquid phase modifies the solute distribution at the grain boundary, which in turn affects the overgrowth mechanism of converging dendrites. We show that there exists a critical melt velocity to determine the growth competition at the grain boundary. In addition, the role of interfacial anisotropy on growth competition is analyzed in detail, where we discern that the conventional overgrowth behavior is dominant at large anisotropic strengths. Lastly, a morphological selection map is depicted to predict the crossover region between the two overgrowth behaviors.

1. Introduction

Over the last few decades the directional solidification (DS) of metallic alloys has garnered interest in industrial and academic appli cations [1 3]. The most common and fundamental structure in a cast product is dendritic in nature, and depending on the interplay between heat and solute, a wide range of oriented dendritic grains is produced. Especially in a polycrystalline sample, the misaligned dendrites interact and compete with each other to affect the microstructural and crys tallographic hallmarks of a cast alloy. Henceforth, in order to improve the applicability, and to understand the structural evolution, several studies [4 9] have been devoted to scrutinize the mechanism of grain selection in misoriented columnar dendrites.

At first, the classical overgrowth model by Walton and Chalmers [4] addressed the dendritic growth competition in converging and diver ging crystals. When two grains converged at the grain boundary (GB), the model predicted that a favorably oriented (FO) dendrite shall overgrow an unfavorably oriented (UO) one. Predominantly, the den drites that evolve along the direction of heat flow are called as FO dendrites, and the ones that grow with a finite inclination with respect to the growth direction are termed as UO dendrites, as schematically illustrated in Fig. 1. Walton and Chalmers suggested that the UO den drites typically require a relatively large undercooling to keep up with the position of a FO dendrite, and therefore the persistent lag of a misoriented dendrite results in the overgrowth of a FO dendrite. This largely accepted overgrowth model was later reported by Rappaz et al. [5,8], where an UO dendrite was sequentially blocked by the primary arms of a favorably oriented dendrite. Additionally, in the case of grains diverging at the grain boundary, the development of secondary and tertiary branches in FO dendrites was regarded as the driving factor to eliminate an UO dendrite.

A few investigations [9 13] have proposed other possible over growth mechanisms for competitive dendrites. Zhou et al. [9] per formed bicrystal experiments on Ni based superalloys and concluded that the growth behavior of converging dendrites is anomalous. It was reported that the solute interaction at the grain boundary has a sig nificant impact on the overgrowth mechanism, where the UO dendrites overgrow at the expense of FO dendrites. This phenomenon referred to

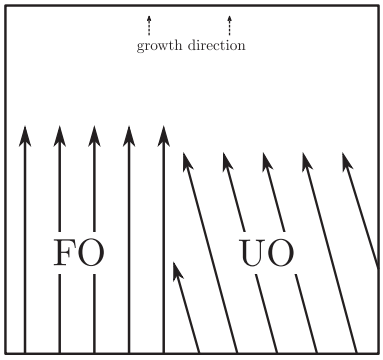

Fig. 1. A schematic illustration of dendritic growth competition at the grain boundary. Here, in accordance with the Walton and Chalmers model [4], a conventional overgrowth phenomenon is showcased where the favorably oriented (FO) dendrites overgrow the unfavorably oriented dendrites at the grain boundary. For the sake of schematic representation, each arrow indicates a single columnar dendrite.

as 'unusual overgrowth' eliminates a favorably oriented dendrite by physically blocking and protruding over the primary arms. Furthermore, other experimental studies [10,12,13] have also endorsed the overgrowth of misoriented dendrites at the grain boundary.

Although erstwhile studies have shed light on the growth behaviors of converging dendrites, the deterministic mechanism of an unusual overgrowth event is yet to be addressed. For many years, the phase field method [14,15] has been an ideal tool to investigate and mimic the growth dynamics of complex dendritic microstructures. Numerous studies [16 19] have examined and depicted the dendritic growth competition in binary alloys. For example, Tourret et al. [16] argued that the growth competition in columnar dendrites was dependent on the imposed temperature gradient, and the rate of suppression of UO dendrites was non monotonic. In addition, for diverging dendrites, it was suggested that the formation of secondary and tertiary arms was always accountable for the overgrowth of favorably oriented dendrites, thereby reiterating the importance of microscopic thermal fluctuations at the interface.

Nevertheless, especially for a converging dendritic network, Li et al. [17] performed phase field simulations in two dimensions and examined the unusual overgrowth behavior at the GB. In tune with the aforementioned experimental observations, it was concluded that the solute interaction at low pulling velocities was responsible for the overgrowth of an unfavorably oriented dendrite. These observations were further acknowledged by Takaki et al. [20], where the unusual overgrowth phenomenon was observed as a result of asymmetric diffusion layers at the grain boundary. In the aforementioned phase field studies, although the unusual overgrowth behavior was addressed during the unidirectional solidification of columnar dendrites, the influence of liquid phase convection was not taken into consideration. Several phase field studies and experiments [21 24] have reported that the inclusion of melt flow in the system completely modifies the solute ahead of the solid liquid interface. Especially, since the solute interaction at the grain boundary is a key factor, the role of melt convection remains an open question. Likewise, the dendritic overgrowth mechanism in the presence of melt flow is less understood in alloy solidification. Henceforth, in the present study, we simulate the competitive growth of dendrites converging at the grain boundary under convective conditions for an isothermal binary alloy model system. Following the introduction, we briefly describe the set of governing equations from our phase field model. In the results and discussion section, we illustrate and highlight different overgrowth mechanisms via two dimensional growth competition of columnar dendrites with and without melt convection. Our results suggest that the presence of melt flow seemingly modifies the overgrowth behavior at the GB. Later, we elucidate the role of interfacial anisotropy on the overgrowth mechanism and the dendritic morphology. The last section is devoted to discussing the conclusions from the present work and possible open questions.

2. Model description

We study the role of liquid phase convection on columnar dendrites by employing a quantitative multiphase field model developed by Choudhury and Nestler [25]. In the last few years several directional solidification studies [26 28] have been performed to address the pattern formation in directionally solidified microstructures. In this model, the phase evolution is determined by the phenomenological minimization of the functional $d\Omega/dt \leqslant 0$, which is formulated as the grand potential functional,

$$\Omega(T, \boldsymbol{\mu}, \boldsymbol{\phi}) = \int_{\Omega} \left[\Psi(T, \boldsymbol{\mu}, \boldsymbol{\phi}) + \left(\epsilon\, a(\boldsymbol{\phi}, \nabla\boldsymbol{\phi}) + \frac{1}{\epsilon} w(\boldsymbol{\phi}) \right) \right] d\Omega. \tag{1}$$

Here, $\boldsymbol{\mu} = (\mu_i, \ldots, \mu_{K-1})$ is a vector consisting of $K-1$ chemical potentials of the system at a given temperature and $\boldsymbol{\phi} = (\phi_\alpha, \ldots, \phi_N)$ describes the phase vector with ϕ_α being the local volume fraction of the phase α. ϵ is a length scale related to the width of the diffuse interface. In this model, K represents the total number of components in the system, T is the temperature and N is the total number of phases in the system. $\epsilon\, a(\boldsymbol{\phi}, \nabla\boldsymbol{\phi})$ and $\frac{1}{\epsilon} w(\boldsymbol{\phi})$ are the gradient and obstacle potential type energy densities [29]. The grand potential density $\Psi(T, \boldsymbol{\mu}, \boldsymbol{\phi})$ is the Legendre transform of the free energy density of the system $f(T, \boldsymbol{c}, \boldsymbol{\phi})$, where $\boldsymbol{c}$ is the concentration vector, expressed as the interpolation of individual grand potential densities Ψ_α

$$\Psi(T, \boldsymbol{\mu}, \boldsymbol{\phi}) = \sum_{\alpha=1}^{N} \Psi_\alpha(T, \boldsymbol{\mu}) h(\phi_\alpha), \tag{2}$$

with,

$$\Psi_\alpha(T, \boldsymbol{\mu}) = f_\alpha(\boldsymbol{c}^\alpha(\boldsymbol{\mu}, T), T) - \sum_{i=1}^{K-1} \mu_i c_i^\alpha(\boldsymbol{\mu}, T). \tag{3}$$

For a multi phase field representation, the interpolation function $h(\phi_\alpha)$ is of the form

$$h(\phi_\alpha) = \frac{\widetilde{h}(\phi_\alpha)}{\sum_{\beta} \widetilde{h}(\phi_\beta)}, \tag{4}$$

ensuring that the condition $\sum_\beta h(\phi_\beta) = 1$ is always fulfilled [30]. $\widetilde{h}(\phi_\alpha)$ is expressed as a higher order polynomial

$$\widetilde{h}(\phi_\alpha) = \phi_\alpha^2(3 - 2\phi_\alpha). \tag{5}$$

In order to describe the thermodynamics of the respective bulk phases of a binary isothermal model alloy system, we approximate the variation of the grand potential of the respective phases using a second degree polynomial for a model binary alloy system in a method proposed by Choudhury [31]. Here, the equilibrium mole fractions of component j in the solid α and the liquid β are set as $c_j^{\alpha,\mathrm{eq}} = 0.2$ and $c_j^{\beta,\mathrm{eq}} = 0.8$ respectively. Also, the dimensionless melt supersaturation Δ is given as

$$\Delta = \frac{c_j^{\beta,\mathrm{eq}} - c_j^{\beta}}{c_j^{\beta,\mathrm{eq}} - c_j^{\alpha,\mathrm{eq}}}, \tag{6}$$

where c_j^β is the initial melt concentration in liquid phase. Additionally, for any other binary alloy system, the equilibrium concentrations and the melt supersaturation in Table 1 should be selected accordingly.

Furthermore, the gradient energy in Eq. (1) is expressed as

$$a(\boldsymbol{\phi}, \nabla\boldsymbol{\phi}) = \sum_{\alpha,\beta=1}^{N,N} \gamma_{\alpha\beta} [a_c(\boldsymbol{q}_{\alpha\beta})^2] |\boldsymbol{q}_{\alpha\beta}|^2, \tag{7}$$

Table 1
Material and simulation parameters.

Description	Parameter	Value
Diffusivity	D^{β}	1.00
Partition coefficient	k	0.25
Melt supersaturation	Δ	0.525
Fluid density	ρ	1.00
Dynamic viscosity	η	1.00
Interface width	ϵ	4.00
Discretized grid space	$\Delta x = \Delta y$	1.00

where $\gamma_{\alpha\beta}$ is the interfacial free energy per unit area of the α/β phase boundary. The generalized antisymmetric gradient vector $\boldsymbol{q}_{\alpha\beta}$ reads $\boldsymbol{q}_{\alpha\beta} = \phi_{\alpha}\nabla\phi_{\beta} - \phi_{\beta}\nabla\phi_{\alpha}$. In the present model, a cubic symmetry is mod elled via the expression

$$a_{\alpha\beta}(\boldsymbol{q}_{\alpha\beta}) = 1 - \delta_{\alpha\beta}\left(3 \mp 4\frac{|\boldsymbol{q}_{\alpha\beta}|_4^4}{|\boldsymbol{q}_{\alpha\beta}|^4}\right). \tag{8}$$

Here, the strength of the anisotropy of an α/β interface is given by the parameter $\delta_{\alpha\beta}$. In the present study, the axial tilt of individual grains with respect to the growth direction aligned along the y axis and ro tation are used to define the crystal misorientation. Hence, the crystal reference frame can be rotated by an angle with respect to the la boratory frame and this allows us to explore different relative or ientations of the equilibrium solid liquid interfaces with respect to the growth direction. The multiobstacle type potential is of the form

$$w(\boldsymbol{\phi}) = \frac{16}{\pi^2}\sum_{\alpha<\beta}\gamma_{\alpha\beta}\phi_{\alpha}\phi_{\beta}. \tag{9}$$

The evolution equation for N phase field variables is written as

$$\tau\epsilon\frac{\partial\phi_{\alpha}}{\partial t} = \epsilon\left(\nabla\cdot\frac{\partial a(\boldsymbol{\phi},\nabla\boldsymbol{\phi})}{\partial\nabla\phi_{\alpha}} - \frac{\partial a(\boldsymbol{\phi},\nabla\boldsymbol{\phi})}{\partial\phi_{\alpha}}\right) - \frac{1}{\epsilon}\frac{\partial w(\boldsymbol{\phi})}{\partial\phi_{\alpha}} - \frac{\partial\Psi(T,\boldsymbol{\mu},\boldsymbol{\phi})}{\partial\phi_{\alpha}} - \Lambda, \tag{10}$$

where Λ is a Lagrange multiplier so that the local constraint $\sum_{\alpha=1}^{N}\phi_{\alpha} = 1$ is fulfilled. The relaxation constant τ is chosen according to the ex pression in Ref. [25], such that the attachment kinetics at the interface vanishes.

The evolution equation for the chemical potentials is written as

$$\frac{\partial\mu_i}{\partial t} = \sum_{i,j=1}^{K-1}\left[\sum_{\alpha=1}^{N}h(\phi_{\alpha})\frac{\partial c_i^{\alpha}(\boldsymbol{\mu})}{\partial\mu_j}\right]_{ij}^{-1}\times\left\{\nabla\cdot\sum_{i,j=1}^{K-1}(M_{ij}(\boldsymbol{\phi})\nabla\mu_j - \mathbf{U}c_i - \boldsymbol{J}_{at} - \boldsymbol{q}) - \sum_{\alpha=1}^{N}c_i^{\alpha}(\boldsymbol{\mu})h'(\phi_{\alpha})\frac{\partial\boldsymbol{\phi}}{\partial t}\right\}. \tag{11}$$

The right hand side has contributions from diffusion as a result of gradients in the chemical potential, the interface mobility $M_{ij}(\boldsymbol{\phi})$ is defined in [29], and $\mathbf{U}$ is the liquid velocity vector. The term '$\boldsymbol{q}$' in Eq. (11) is introduced to account for the thermal fluctuations in our si mulations, and $\boldsymbol{J}_{at}$ represents the corrective anti trapping term that produces a mass flux along the normal direction, and thereby coun terbalances the trapping current due to the presence of non equilibrium artifacts such as the solute trapping [25,32].

Furthermore, the fluid momemtum and mass conservation equa tions are given as

$$\rho\left(\frac{\partial}{\partial t}(\phi_{\beta}\mathbf{U}_{\beta}) + \phi_{\beta}\mathbf{U}_{\beta}\cdot\nabla\mathbf{U}_{\beta}\right) = -\phi_{\beta}\nabla p + \nabla\cdot[\eta(\nabla\phi_{\beta}\mathbf{U}_{\beta} + \nabla\phi_{\beta}\mathbf{U}_{\beta}^{T})] - \boldsymbol{M}_l^d, \tag{12}$$

and

$$\nabla\cdot(\phi_{\beta}\mathbf{U}_{\beta}) = 0. \tag{13}$$

Here ρ, p, η denote the density, pressure and the dynamic viscosity of the liquid alloy melt respectively. In the present phase field study, we introduce a non conserved quantity ϕ_{β} for the liquid phase and ϕ_{α} for solid, $\phi_{\alpha} = 1 - \phi_{\beta}$, on the basis of the local constraint $\sum_{\alpha=1}^{N}\phi_{\alpha} = 1$. The momentum equation as a function of the phase field vector $\boldsymbol{\phi}$ is based on the Beckermann model [21] and similar to other phase field studies [22,33]. The above formulation is generally employed for phase field simulations coupled with convection in the liquid melt. Generally the velocity vector is expressed as $\mathbf{U} = \phi_{\alpha}\mathbf{U}_{\alpha} + \phi_{\beta}\mathbf{U}_{\beta}$, and since the solid phase is considered stationary and rigid $\phi_{\alpha}\mathbf{U}_{\alpha} = 0$, the melt velocity is expressed as $\mathbf{U} = \phi_{\beta}\mathbf{U}_{\beta}$. Again, similar to Beckermann [21], the last term $\boldsymbol{M}_l^d$ explains the dissipative viscous stress, expressed as

$$\boldsymbol{M}_l^d = \eta h\boldsymbol{\phi}_{\beta}\frac{\mathbf{U}}{\epsilon}|\nabla\phi_{\beta}|, \tag{14}$$

Here, h is the dimensionless parameter. This particular term provides a distributed momentum sink in the diffuse interface region, thus forcing the liquid velocity to zero as $\phi \to 1$, such that while approaching to wards the liquid side, the velocity vector becomes linear. The dis sipative term plays a fundamental role in smoothening the velocity profile for a wide range of diffuse interface thickness ϵ. The di mensionless parameter h is generally evaluated via performing an asymptotic analysis and in the present model, h has the value 7.989 for the obstacle type potential Eq. (9). In total, the Eqs. (13), (11), and (12) incorporate the melt convection in our grand potential formulation [25]. The above equations are solved using a finite discretization on a staggered mesh and the time derivative follows an explicit Euler scheme. The current numerical algorithm is parallelized via message passing interface (MPI).

3. Initial and boundary conditions

In the present study, the competitive growth of columnar dendrites in the presence of melt convection is simulated in two dimensions. As shown in Fig. 2, a computational domain of $1000\Delta x \times 750\Delta y$ numerical cells is selected, where $\Delta x = \Delta y = 1.0$. As an initial condition and in a uniformly supersaturated melt, the simulation starts with 10 spherical seeds at the bottom of the domain. Depicted in blue and green colors in Fig. 2, the first five seeds are named as favorably oriented (FO) den drites with $\theta_{FO} = 0°$, whereas, the next five seeds are called unfavorably oriented (UO) dendrites, inclined at $\theta_{UO} = 15°$ in the anticlockwise di rection with respect to the growth direction. Here, the crystal orienta tion along the y direction is defined as $\theta_0 = 0°$, and the anticlockwise direction is taken as positive. Based on their orientation and position, all the spherical seeds have been numbered accordingly in Fig. 2. Since the present study explores the role of liquid phase convection, the in itial distance between the spherical seeds is kept constant for all the simulations. The boundary conditions for the left and right side of the simulation domain is considered periodic for all the fields. The lateral melt flow is introduced from the left boundary wall and travels along the horizontal direction. In addition, on the top and bottom sides, the Neumann boundary condition is applied for the phase and solutal fields, whereas, a slip condition is applied for the velocity fields. In order to simulate the columnar dendrites in the domain for a long time period, a moving frame method [34] is applied when the total number of cells between the foremost solid liquid interface and the top boundary is less than 450 numerical cells. Thereafter, for every time step, the bottom cells along the y direction are shifted downwards and cutoff. This method generally saves time and computational effort, and also ensures that the concentration fields are unaffected by the boundary conditions.

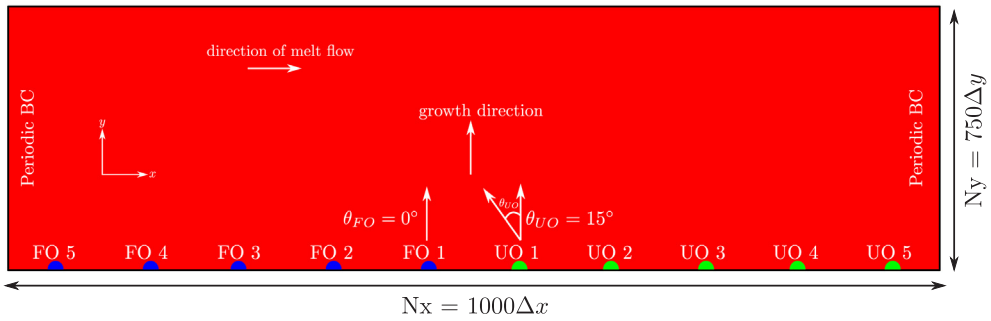

Fig. 2. Schematic illustration of the simulation setup along with the imposed initial and boundary conditions. Ten equidistant spherical seeds are initialized in a supersaturated melt of composition Δ. Here, the blue seeds are oriented favorably along the growth direction at $\theta_{FO} = 0°$, whereas, the unfavorably oriented seeds green in color are misoriented at $\theta_{UO} = 15°$ in the anticlockwise direction. (For interpretation of the references to colour in this figure legend, the reader is referred to the web version of this article.)

4. Results and discussion

4.1. Growth competition of columnar dendrites

Firstly, a two dimensional competitive growth of converging dendrites is simulated in the absence of convection. During the progressive solidification of a dendritic network in Fig. 3(a), we observe that the favorably oriented dendrites overgrow the unfavorably oriented dendrites over a period of time. A detailed time lapse of the concentration fields in Fig. 3(b) (e) depicts the overgrowth mechanism of columnar dendrites at the grain boundary. At $t = 1000$ in Fig. 3(b), we found that the tip position of the dendrite UO1 is already behind the FO1 dendrite. As the solidifying front advances, the dendrite FO1 migrates towards the UO1 dendrite without producing large and amplified secondary arms, such that the GB orientation remains in parallel to the FO1 dendrite. Consequently, the inter dendritic spacing decreases and the position of the UO1 dendrite tip rapidly descends. After the elimination of an unfavorably oriented primary arm, the dendrite FO1 now becomes a GB dendrite, as schematically denoted in Fig. 3(a). Such an overgrowth phenomenon usually happens due to the overlap of the concentration fields at the grain boundary and the difference in the tip undercooling between the FO1 and UO1 dendrites. Since the position of the tips differ and the lag of a misaligned dendrite is significant, the UO1 dendrite is always blocked by the primary arm of the FO1 dendrite. Besides, as reported in a previous study [20], we believe that the rate of elimination of an UO dendrite also increases with an increase in the orientation angle of UO dendrites.

The present observation, widely known as the conventional overgrowth phenomenon is corroborated by the classical dendritic overgrowth theory of Walton and Chalmers [4], where the FO dendrites overgrew as a consequence of low undercooling at the tip position. Furthermore, as described in a recent phase field study [17], the aforementioned overgrowth phenomenon is independent of the initial seed spacing. Since the migration of an UO dendrite is principally towards a nearby FO dendrite, its spacing with an adjacent neighbour decreases, and hereafter the dendrite is invariably blocked.

4.2. Influence of melt convection

In the present section, the microstructural evolution of converging dendrites is systematically investigated when diffusion and convection are both contemplated. The direction of the imposed melt flow is perpendicular to the dendritic growth direction from the left to the right boundary. The first two microstructures in Fig. 4 represent the competitive growth of columnar dendrites at low melt velocities, $U_x = 1.0 \times 10^{-1}$ to $U_x = 1.5 \times 10^{-1}$, where U_x is the magnitude of convection velocity along the x direction. In a similar way to the observation in the previous section, from the outset, the FO1 dendrite primary arm blocks the UO1 dendrite, and consequently dominates the growth competition. This impingement of FO and UO dendrites at low melt velocities is associated with the conventional overgrowth phenomenon, and accordingly, the effect of melt flow is marginally noticed,

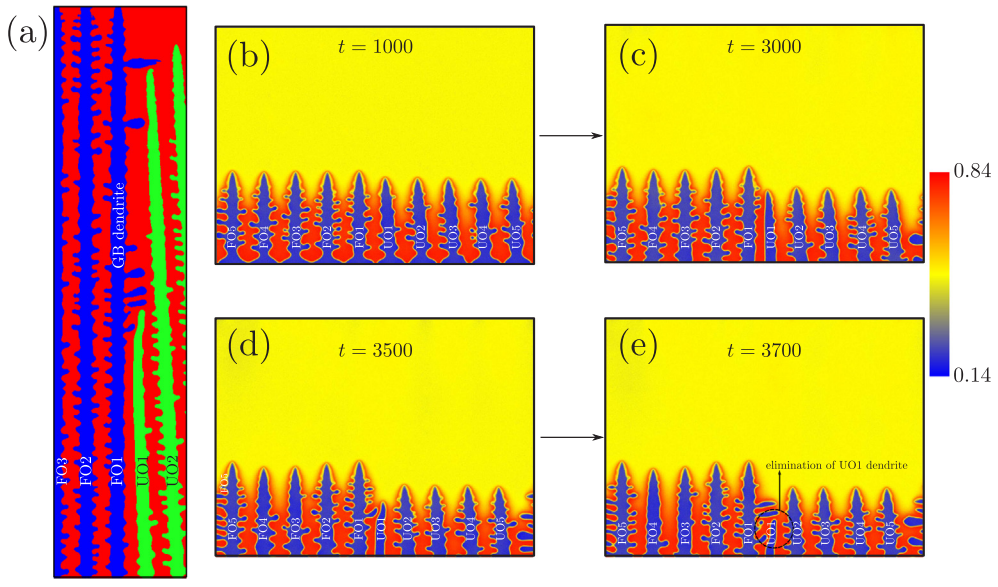

Fig. 3. (a) Under pure diffusive conditions, reconstructed simulation snapshots demonstrate the growth competition of columnar dendrites converging at the grain boundary. Here, the FO dendrites are represented by the blue color, whereas the green color represent the UO dendrites. (b)–(e) The temporal evolution of dendritic morphologies in a supersaturated melt, where the FO1 dendrite impinges and subsequently blocks the primary arm of the UO1 dendrite. The color bar illustrates the concentration field according to the legend embedded adjacent to the snapshots. This dendritic overgrowth behavior at the grain boundary is widely known as the conventional overgrowth phenomenon. Highlighted in Fig. 3(a), the dendrites that overgrow and dictate the growth process at the grain boundary are named as 'GB dendrite'. (For interpretation of the references to colour in this figure legend, the reader is referred to the web version of this article.)

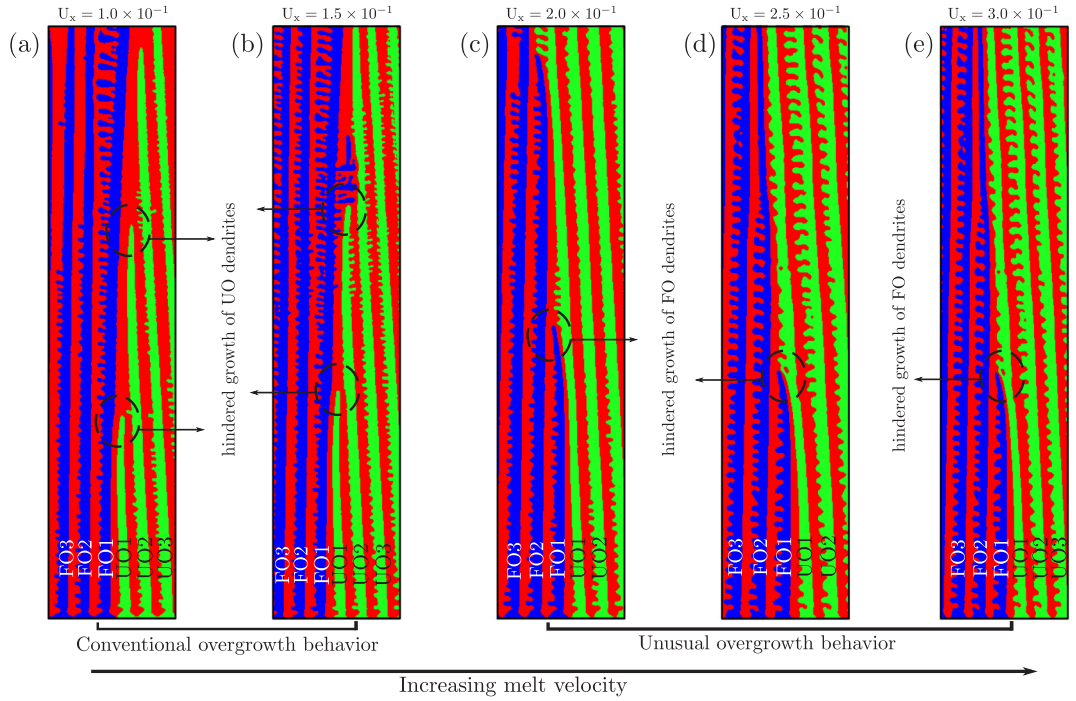

Fig. 4. (a)–(e) Competitive growth of converging columnar dendrites under the influence of melt convection. The conventional overgrowth behavior transforms into an unusual overgrowth behavior as the liquid alloy melt velocity is gradually increased. (a) and (b) While the FO1 dendrite dominates the growth competition up to $U_x = 1.5 \times 10^{-1}$, (c)–(e) the UO1 dendrite overgrows and sequentially eliminates the favorably oriented dendrites at high melt velocities. The lateral migration of the converging grain boundary towards the upstream direction (left direction) is observed for $U_x > 1.5 \times 10^{-1}$. The overgrowth events are highlighted schematically for each case. Here, the FO dendrites are represented by the blue color, whereas the green color represents the UO dendrites.

where the solidification front deflects the primary trucks towards the downstream (right) direction, see Fig. 4(a) and (b). Since the evolution of the FO1 dendrite is controlled by the imposed anisotropy under pure diffusive regime, the lateral tilt is completely absent, however, the presence of a convective transport mechanism near the solidifying front tilts the FO1 dendrite arm along the flow direction. Consistent with previous studies [35,36], the solutal gradients are weakened as a result of an overgrowth event, and the solute distribution near the FO1 tip shifts entirely along the flow direction, thereby causing different tilting modes under diffusive convective regime.

Next, with an increase in the melt velocity, i.e., from $U_x = 1.5 \times 10^{-1}$ to 3.0×10^{-1}, the overgrowth behavior at the grain boundary is unconventional. Illustrated in Fig. 4(c) (e), the unfavorably oriented dendrites with $\theta_{UO} = 15°$ overgrow at the expense of FO dendrites. From Fig. 4(c) (e), we notice that the primary arm of the UO1 dendrite converges at the GB and sequentially retards the growth of the FO1 dendrite. This anomalous behavior of converging dendrites in Fig. 4(c) (e), namely, the unusual overgrowth phenomenon [9,11], has been primarily observed in various experimental [9,11,12] and phase field studies [18,20,17]. The in situ findings of D'souza et al. [11] and Zhou et al. [9] argued and concluded that a misoriented dendrite shall indeed overgrow at the expense of a well oriented columnar dendrite. Their results proposed that the solute interaction at the grain boundary played a key role during the dendritic growth competition, which was neglected in the earlier overgrowth models [4,7,8]. To the best of our knowledge, this overgrowth transition from the conventional growth to the unusual growth in a bicrystal dendritic network has never been reported before, especially in the presence of melt convection.

The dendritic growth competition is further interpreted in Fig. 5, where the temporal volume fractions of favorably and unfavorably oriented grains are illustrated at $U_x = 1.0 \times 10^{-1}$ and $U_x = 2.5 \times 10^{-1}$, respectively. The dominance of FO dendrites (no misorientation) in a conventional overgrowth phenomenon is depicted in Fig. 5(a), where the grain volume fraction diverges after the initial stages of columnar solidification. After the first conventional overgrowth event at the grain boundary, the favorably oriented dendrites dominate the growth competition as a result of physically protruding and blocking the primary arms of UO dendrites. In contrast, due to successive unusual overgrowth events at the grain boundary, the volume fraction of an UO grain overtakes the FO dendritic grain in Fig. 5(b). Since the UO1 dendrite drifts towards the grain boundary to suppress a favorably oriented dendrite, the unfavorably oriented volume fraction increases with time. The distance between the UO1 and the FO1 dendrite tip position increases with the misorientation angle such that the leading FO1 dendrite continuously blocks the lagging UO dendrites with time. As a result, the volume fractions of UO dendrites diverge immediately in a conventional overgrowth. In contrast, the solutal layer near the UO1 tip becomes thinner and the UO1 dendrite overcomes the leading FO1 dendrite in an unusual overgrowth model. In order to travel laterally towards the converging grain boundary and to overgrow a FO dendrite, the time taken by the UO1 dendrite increases, and therefore the temporal volume fractions diverge during the later stages of inter dendritic growth competition. The small peaks at different time steps in Fig. 5(b) indicate the impingement of the UO1 dendrite with different favorably oriented dendrites at the converging grain boundary. Once, the overgrowth mechanism is entrenched at the grain boundary, the GB dendrite dictates the growth competition. In both overgrowth behaviors, the diverging nature of volume fractions indicates the individual dominance during the inter dendritic growth competition.

Next, when the UO1 dendrite travels laterally across the grain boundary, the drift velocity of the primary arm is calculated as

$$V_d = \left| \frac{dx_t}{dt} \right| \tag{15}$$

where, x_t is the position of the UO1 arm along the x axis, and t is the solidification time. As shown in Fig. 6, an analytical fit provides us with a relationship $V_d^{avg} \propto Pe_f$, where, $Pe_f = U_x L/2D^{\beta}$ is the flow Peclet

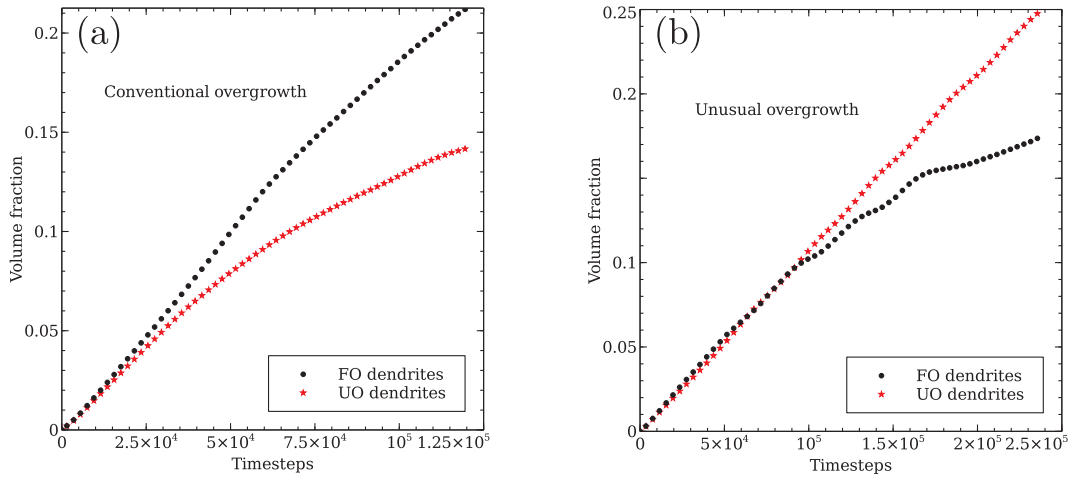

Fig. 5. (a) and (b) Comparative temporal volume fractions of favorably and unfavorably oriented grains at the grain boundary. (a) At $U_x = 1.0 \times 10^{-1}$, the diverging point for each case indicates the most preferred and dominant grain during the dendritic growth competition. FO dendrites dominate growth competition in a conventional overgrowth behavior, while the unfavorably oriented dendrites at $U_x = 2.5 \times 10^{-1}$ protrude consistently to outgrow the FO dendrites during an unusual overgrowth phenomenon at the grain boundary.

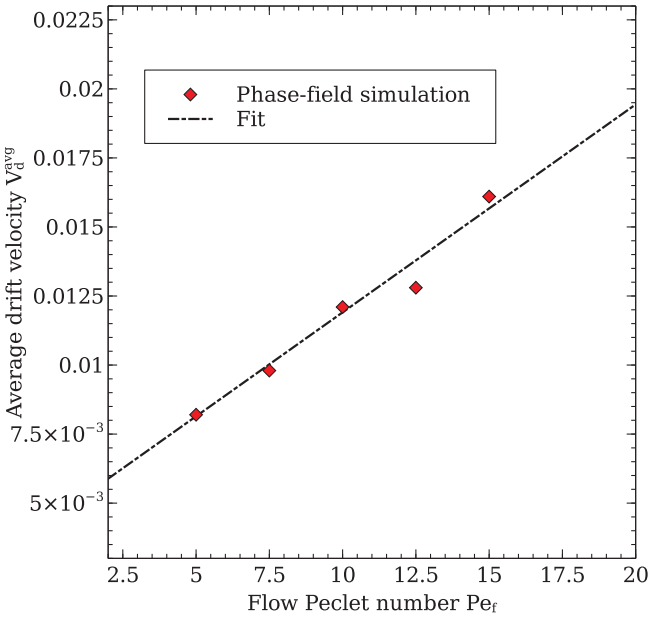

Fig. 6. Average drift velocity of the UO1 primary arm as a function of flow Peclet number. The presence of strong convection velocities leads to faster displacement of UO1 dendrite arm towards the inflow direction, which results in an unusual overgrowth phenomenon at the grain boundary. A linear fit follows the relation $V_d^{avg} = n_1 * Pe_f + n_2$, where n_1 and n_2 are proportionality constants.

number, L is the reference length (inter seed spacing), and V_d^{avg} is the drift velocity averaged across the simulation time. In Fig. 6, we observe that the average drift velocity of the UO1 primary arm increases linearly with an increase in the flow Peclet number. During a conventional overgrowth behavior, the FO1 outgrows laterally at the grain boundary and the UO1 dendrite significantly lags behind. In contrast, a considerable increase in the average drift velocity indicates that the displacement of the unfavorably oriented primary arm towards the inflow direction is larger than its counterpart, which in turn translates to an unusual overgrowth event at the grain boundary. With time, the UO1 dendrite lateral drift towards the regions of higher chemical potential gradients results in the systematic elimination of an individual FO dendrite at the grain boundary. This linearity of the drift velocity shows that the advected solute has a significant role on the overgrowth behavior among converging dendrites.

Likewise, from the present set of simulations, it is noteworthy that the minute secondary and tertiary branches play no major role in the overgrowth mechanism, and thus far the imposed numerical noise has no influence on the growth competition. Again, as mentioned in the previous section, the unusual growth phenomenon shown here does not depend on the inter dendritic spacing, and therefore a FO dendrite shall always be eliminated for conditions greater than the melt velocities $U_x > 1.5 \times 10^{-1}$.

It is important to note that the above set of two dimensional simulations are performed at a fixed misorientation angle $\theta_{UO} = 15°$, and we believe that the critical velocity to predict the overgrowth behavior depends on the inclination angle of the UO dendrites. In this regard, a microstructural selection map is illustrated in Fig. 7, wherein several simulations with different misorientation angles θ_{UO} and flow Peclet numbers Pe_f are performed and represented with colored dots. Here, the unusual overgrowth phenomenon is restricted to higher flow Peclet numbers and lower misorientation angles only. On the other hand, we observe that the conventional overgrowth region increases with an increase in the inclination angle of the unfavorably oriented dendrites. As the imposed misorientation restricts the inclination of the UO1 dendritic tip towards the grain boundary, the growth competition results in the elimination of an unfavorably oriented dendrite. Henceforth, the critical convection velocity to predict the transition between the two overgrowth behaviors increases with the increase in the misorientation angle θ_{UO}, and for $\theta_{UO} \geqslant 20°$, the conventional overgrowth behavior is always observed at the grain boundary.

4.3. *Unusual overgrowth mechanism*

From the above two dimensional simulations, it is evident that the convection in the liquid phase modifies the overgrowth mechanism at the grain boundary. Therefore, in the present section, we analyze in detail the unusual overgrowth phenomenon during the competitive growth of converging dendrites. Figs. 8 and 9 portray the solutal and velocity fields of FO and UO dendrites at low and high melt velocities, respectively. Due to the presence of an additional mass transport, the amount of solute advected varies, and as illustrated at $t = 3000$, the concentration fields near the solidification front are different in Figs. 8 and 9 and 9(a). At $U_x = 1.0 \times 10^{-1}$, the FO1 dendrite is already ahead of the UO1 dendrite, and since the rate of evolution of the UO1 dendrite is much lower than the FO1 dendrite, the UO1 dendrite is consequently blocked by the FO1 dendrite primary arm. In contrast, due to the

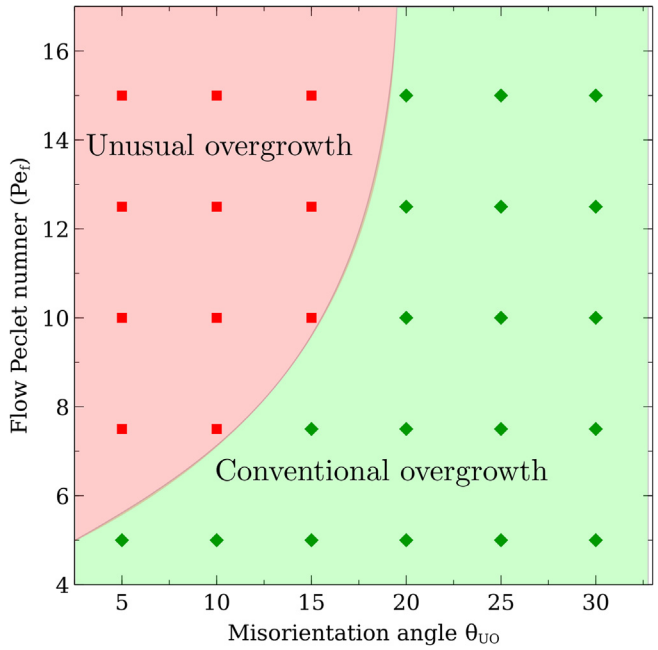

Fig. 7. A microstructural selection map for various misorientation angle θ_{UO} and flow Peclet numbers Pe_f. The unusual overgrowth mechanism is limited within a narrow range, and for $\theta_{UO} > 15°$, the conventional overgrowth behavior dominates at the grain boundary. The transition between the two overgrowth mechanisms is sketched schematically, and does not represent a sharp division.

imposed misorientation $\theta_{UO} = 15°$, the UO1 dendrite initially falls behind the FO1 dendrite tip in Fig. 9. However, on account of the high convection velocity and the resultant solute, the relative driving force at the UO1 dendrite tip is high for $U_x = 2.5 \times 10^{-1}$. The enriched solute layer around the unfavorably oriented dendritic network becomes thinner on the upstream direction (left direction), which in turn assists the lateral drift of the UO1 dendrite at the GB. Hereafter, the UO1 dendrite retains its position and eventually outgrows the FO1 dendrite at $t = 3500$ in Fig. 9(b). For an unusual overgrowth behavior in Fig, 9, the dendrite UO1 migrates towards the upstream direction and reduces its inter dendritic spacing with the FO1 dendrite rapidly. Additionally, the lag of a misaligned dendrite is not so large for $U_x = 2.5 \times 10^{-1}$ which compels the UO1 dendrite be also able to overgrow the FO1 dendrite. This behavior is elucidated via the solutal fields ahead of the FO1 and UO1 dendrites in Fig. 10. The contrasting nature of the lateral profiles causes an asymmetric field at the grain boundary, which in turn enforeces a hindered motion of the FO1 dendrite, resulting in an unusual overgrowth event at the GB. The absence of the UO1 concentration peak in Fig. 10 at $U_x = 1.0 \times 10^{-1}$ signifies the lag of the UO1 dendrite.

For both mechanisms, it is interesting to note that the solute movement in between the FO5 FO2 and UO2 UO5 dendrites enhance the formation of asymmetric secondary arms. We observe that the sidebranches are found to be largely favored on the upstream (left) direction of the primary arms and completely suppressed on the other side. The presence of the left to right lateral flow causes a cumulative solute enrichment at the downstream side, which lowers the local undercooling and correspondingly retards the growth of the side arms along the downstream (right) direction.

The unusual overgrowth mechanism in the present work is corroborated by recent investigations [9,10,13], where the overgrowth behavior of converging dendrites was studied for bicrystal samples. From systematic in situ experiments, it was concluded that the growth of a well aligned columnar dendrite was hindered and the dendritic spacing with its immediate neighbour decreased. Similarly, previous phase field investigations [20,17] have also reported the occurrence of an unusual overgrowth phenomenon for binary alloy systems. While the unidirectional solidification study of Li et al. [17] concluded that the modification of diffusion length for GB dendrites at low pulling velocities was influential for the overgrowth of UO dendrites, Takaki et al. [20] analyzed the temporal trajectories of the dendritic tips and reported that the presence of an asymmetric diffusion layer in front of the FO and UO dendrites was responsible for the unusual overgrowth phenomenon among converging dendrites.

4.4. *Effect of interfacial anisotropy*

It has been well known for a long time that the solid liquid interfacial anisotropy is an important parameter to determine the shape of a dendrite [37]. In general, the strength of the imposed anisotropy dictates the morphology and in turn modifies the solutal fields near a dendritic tip. Therefore, since the dendritic growth competition deals with the overlap of the concentration fields at the GB, we briefly study the role of the solid liquid interfacial anisotropy in the present section.

At an imposed melt velocity $U_x = 2.5 \times 10^{-1}$, Fig. 11 illustrates the two dimensional simulations of converging dendrites for different anisotropic strengths $\delta_{\alpha\beta}$. With an increase in the anisotropic strength, we observe that the unusual overgrowth in Fig. 11 translates into a conventional overgrowth phenomenon at the grain boundary. The growth

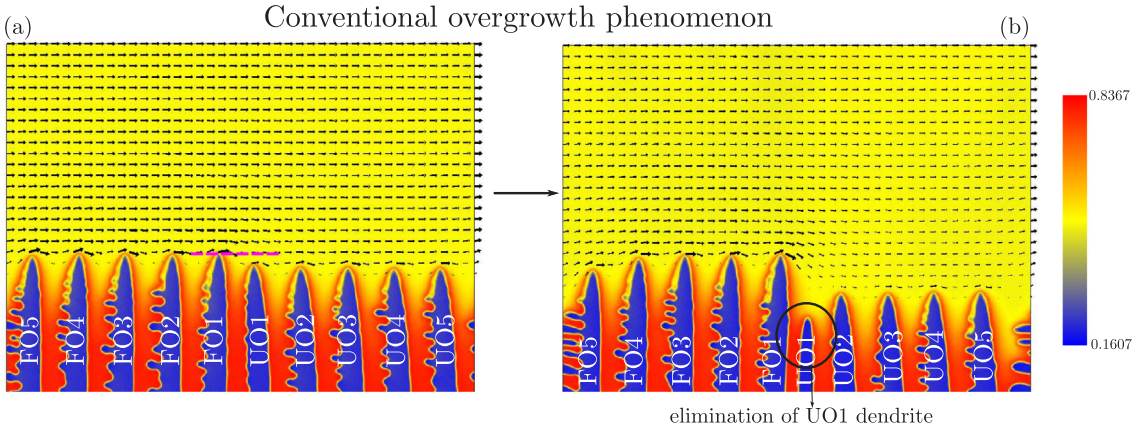

Fig. 8. Concentration and velocity fields of unidirectionally solidified converging columnar dendrites at $U_x = 1.0 \times 10^{-1}$. The FO1 dendrite impinges and eliminates the UO1 dendrite and undergoes the conventional overgrowth mechanism at the grain boundary. The size of the black arrows indicate the magnitude of the velocity fields. The dashed lines near the UO1 and FO1 dendrites indicate the position at which the solutal fields are extracted. The color bar illustrates the concentration field according to the legend embedded adjacent to the snapshots. (For interpretation of the references to colour in this figure legend, the reader is referred to the web version of this article.)

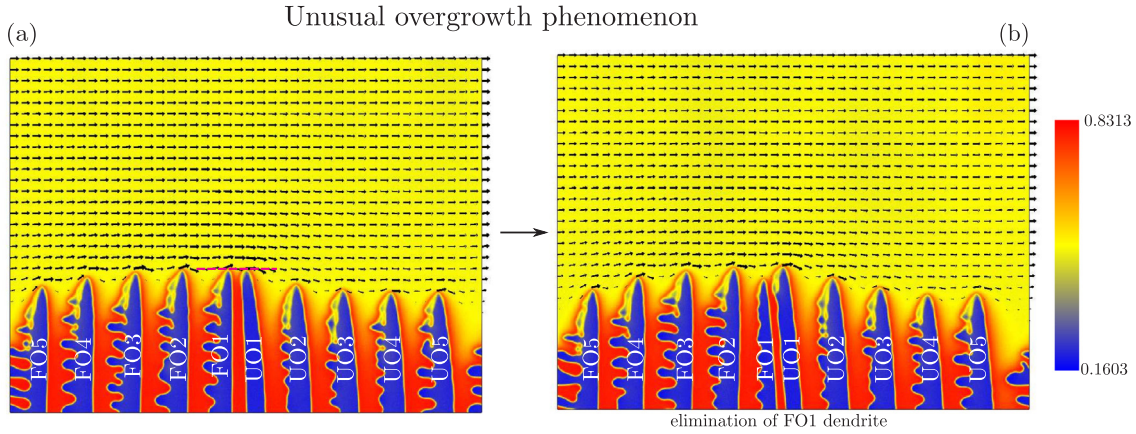

Fig. 9. Concentration and velocity fields of unidirectionally solidified converging columnar dendrite at $U_x = 2.5 \times 10^{-1}$. Here, the UO1 dendrite shifts towards the GB and subsequently eliminates the FO1 dendrite during the course of unidirectional solidification. Since the imposed melt velocity and the amount of advected solute is high, the UO1 dendrite dominates the growth competition at the grain boundary. The lateral shift of the UO1 dendrite towards the inflow direction is significant. The size of the black arrows indicate the magnitude of the velocity fields. The dashed lines near the UO1 and FO1 dendrites indicate the position at which the solutal fields are extracted. The color bar illustrates the concentration field according to the legend embedded adjacent to the snapshots. (For interpretation of the references to colour in this figure legend, the reader is referred to the web version of this article.)

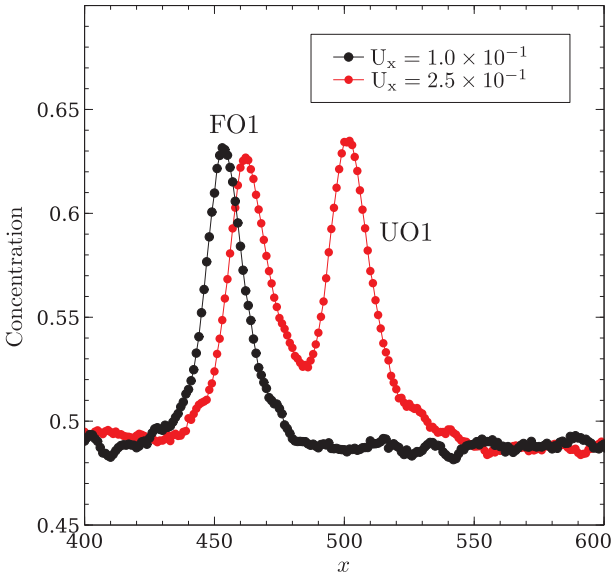

Fig. 10. Lateral solutal profiles near the FO1 and UO1 dendrites at two different convection velocities. Contrasting nature of the advected solute modifies the overgrowth mechanism for converging dendrites at the grain boundary. The small fluctuations indicate the imposed noise in the supersaturated melt.

competition shown in the previous section is recaptured for $\delta_{\alpha\beta} \leqslant 0.04$, where the UO1 dendrite protrudes and retards the primary arm of the FO1 dendrite. However, for $\delta_{\alpha\beta} = 0.05$, a strong crystalline anisotropy in the solid liquid surface energy completely locks the preferred growth direction of the dendritic tips, and henceforth the growth competition is in accordance with the conventional overgrowth model [4]. In uni directional solidification, the advected solute near the solid liquid in terface and the tip shape oversees the behavior of columnar dendrites. At higher $\delta_{\alpha\beta}$, the contribution from the anisotropy in the surface energy dominates, and therefore the dendritic tip responds to the concentra tion field in order to change its growth direction towards the steepest chemical gradient in the supersaturated melt. As a result, the FO1 dendrite arm eliminates an unfavorably oriented dendrite at the grain boundary. The surface energy and advected solute in the melt dyna mically compete with each other to determine the overgrowth me chanism at the grain boundary. Besides, for $\delta_{\alpha\beta} = 0.02$, since the im posed crystalline anisotropy is weak, the flow pattern near the solid liquid interface induces oscillations to the UO1 dendrite tip radius to trigger tip splitting events. Thereafter, any further decrease in the an isotropic strength ($\delta_{\alpha\beta}$) results in the formation of tip splitting dendritic microstructures [28].

Next, the grain boundary orientation θ_{GB} as a function of anisotropic strength is shown in Fig. 12, where θ_{GB} is the inclination angle of the grain boundary with respect to the y direction. An analytical fit pro vides us with the relationship of the form $r_1 + r_2\delta_{\alpha\beta}$, where r_1 and r_2 are proportionality constants. Until $\delta_{\alpha\beta} \leq 0.04$, the grain boundary with an anti clockwise orientation monotonously tilts towards the upstream direction, whereas, at $\delta_{\alpha\beta} = 0.05$, the GB is inclined along the down stream direction as a result of an UO dendrite elimination. In Fig. 11, although the lateral displacement of the GB is profound for weak $\delta_{\alpha\beta}$, a restricted lateral movement of the GB dendrite is noticed for higher anisotropic strengths. The GB orientation systematically goes negative (clockwise direction), which means that well oriented dendrites never get eliminated by misoriented ones. We also observe that the rate at which the UO1 dendrite impinges the favorably oriented dendrites decreases with an increase in the anisotropic strength.

In addition, a microstructural selection map is illustrated in Fig. 13, wherein the overgrowth behaviors are diversified over a wide spectrum of anisotropic strength $\delta_{\alpha\beta}$ and flow Peclet numbers Pe_f. Here, the unusual overgrowth phenomenon is restricted to higher flow Peclet numbers and lower anisotropic strengths only. On the other hand, we observe that the conventional overgrowth region increases with the increase in the anisotropic strength. As the imposed anisotropy restricts the movement of the UO1 dendritic tip towards the upstream direction, the growth competition results in the elimination of an unfavorably oriented dendrite. This tendency to restrict the displacement of the UO1 dendrite decreases with decrease in the anisotropic strength. It is no teworthy that the critical melt velocity to predict the transition between the overgrowth behaviors increases with an increase in the anisotropic strength. We also would like to emphasize that the solid line in Fig. 13 is a schematic division of the two overgrowth mechanisms and not a strict transition zone. Nevertheless, based on the series of simulations, it can henceforth be concluded that the strength of the interfacial aniso tropy also plays a key role in determining the overgrowth mechanism among columnar dendrites at the grain boundary.

5. Conclusions

In this study, we have performed two dimensional phase field si mulations to investigate the growth competition of columnar dendrites

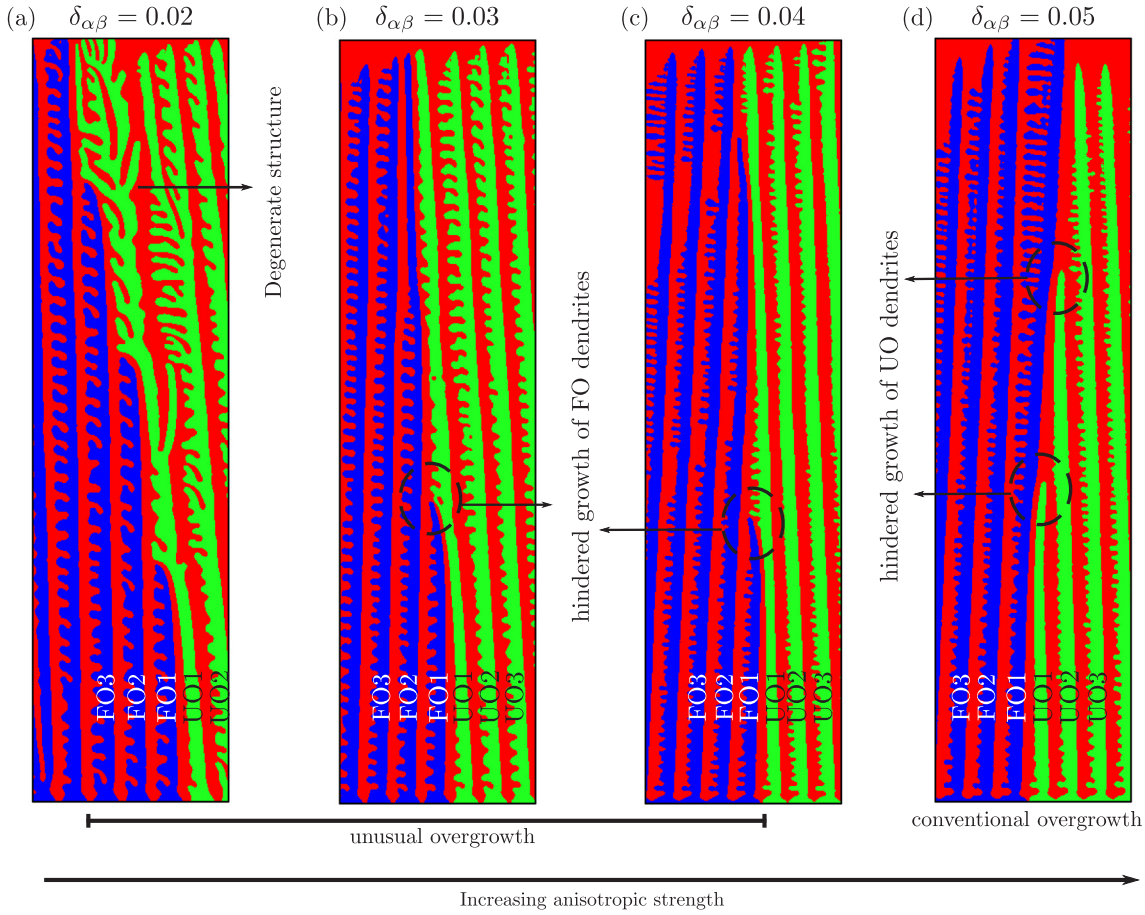

Fig. 11. In unidirectional solidification, the growth competition of columnar dendrites at various anisotropic strengths $\delta_{\alpha\beta}$. The unusual overgrowth phenomenon observed for $\delta_{\alpha\beta} \leq 0.04$ changes to a conventional overgrowth behavior at the grain boundary as the anisotropic strength gradually increases. A degenerate and a tip splitting UO dendrite is generated for weaker anisotropic strengths. Here, the FO dendrites are represented by the blue color, whereas the green color represents the UO dendrites. (For interpretation of the references to colour in this figure legend, the reader is referred to the web version of this article.)

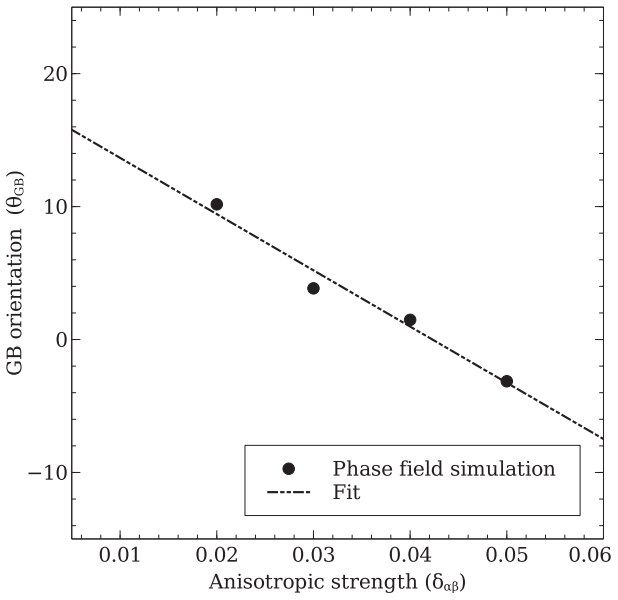

Fig. 12. For $U_x = 2.5 \times 10^{-1}$, the grain boundary orientation (θ_{GB}) at various anisotropic strengths. A linear fit provides us with a relation $\theta_{GB} \propto \delta_{\alpha\beta}$, wherein the by-product of a positive GB orientation is the elimination of a FO dendrite, whereas, a negative GB orientation indicates the overgrowth of FO dendrites.

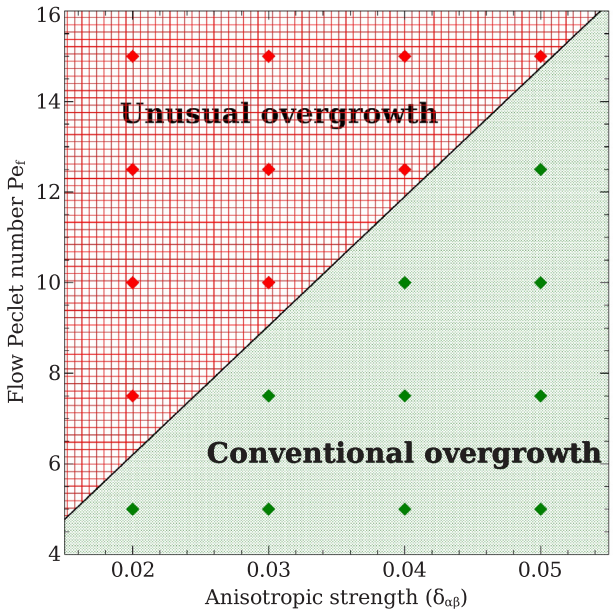

Fig. 13. A microstructural selection map for dendritic growth competition at various combinations of ($\delta_{\alpha\beta}$, Pe_f). While the unusual overgrowth phenomenon dominates at high flow Peclet numbers, an increase in the anisotropic strength produces the widely known conventional overgrowth behavior at the grain boundary. The solid line indicates a schematic transition zone.

in the presence of melt convection. Illustrated in several bicrystal studies, we have captured and analyzed the overgrowth behaviors of columnar dendrites at the grain boundary. Firstly, under pure diffusive conditions, we have shown that the growth competition in converging dendrites follows the classical grain selection mechanism of Walton and Chalmers, where a favorably oriented dendrite impinges and eliminates an unfavorably oriented dendrite at the grain boundary. However, after the introduction of convection in the liquid phase, the overgrowth model translates into an anomalous overgrowth phenomenon. Recognized as an unusual overgrowth behavior, the UO dendrites overgrow at the GB via blocking the primary arms of the FO dendrites. From our series of two dimensional simulations, we conclude that the presence of an additional mass transport in the bulk liquid phase advects the solute near the FO and UO dendrite tips, which in turn modifies the overgrowth mechanism at the grain boundary. The dendritic growth competition is further analyzed via the grain volume fraction and the average drift velocity of the UO1 primary arm. The present findings further broaden our understanding of the overgrowth mechanism under convective conditions, which has been ignored in earlier phase field studies.

The role of interfacial anisotropy on the overgrowth mechanism is also emphasized in the present study. For anisotropic strengths $\delta_{\alpha\beta} \leqslant 0.04$, the unusual overgrowth behavior is observed for columnar dendrites at the grain boundary. A major conclusion is that a strong anisotropic strength $\delta_{\alpha\beta} > 0.04$ locks the direction of the dendritic tips resulting in a conventional overgrowth phenomenon, in accordance with the classical model of Walton and Chalmers. Since the tip shape and the solutal fields near the solidification front are affected, we believe that the contribution from the surface energy restricts the lateral movement of the UO1 dendrite towards the upstream direction. A morphological selection map at various ($\delta_{\alpha\beta}$, $\mathrm{Pe_f}$) is illustrated to depict the transition region between the overgrowth phenomenons at various anisotropic strengths. Our results also indicate that the critical melt velocity to predict the transition between two overgrowth behaviors increases with an increase in the anisotropic strength.

The results shown in the present article can be further extended to a polycrystalline dendritic network with several misoriented grains. Furthermore, since the distance between the columnar dendrites influences the microstructural properties in cast alloys, the prediction of primary dendrite arm spacing (PDAS) is the subject of an ongoing work. Lastly, although the present work provides realistic insights into the overgrowth mechanism, in future, to further enhance our understanding, three dimensional simulations are planned to study the growth competition among columnar dendrites and the role of solute interaction in the presence of fluid flow. In addition, by introducing melt flow in three dimensional dendrite/cell structures, we shall be able to evaluate the realistic permeability in between the primary arms.

Data availability

The raw/processed data required to reproduce these findings cannot be shared at this time as the data also forms part of an ongoing study.

CRediT authorship contribution statement

V. Pavan Laxmipathy: Conceptualization, Methodology, Investigation, Data curation, Software, Validation, Visualization, Writing original draft, Writing review & editing. **Fei Wang:** Writing review & editing. **Michael Selzer:** Writing review & editing. **Britta Nestler:** Resources, Project administration, Funding acquisition, Writing review & editing, Supervision.

Declaration of Competing Interest

The authors declare that they have no known competing financial interests or personal relationships that could have appeared to influence the work reported in this paper.

Acknowledgements

The authors thank the cooperative graduate school “Gefügestrukturanalyse und Prozessbewertung” funded by the ministry of the state of Baden Württemberg (MWK), Germany. Support fo the Helmholtz association through the programmes“Renewable Energies 35.14” and “Virtual Materials Design (VirtMat)” is acknowledged. We are grateful to the computing time of high performance clusters provided by the state of Baden Württemberg through bwHPC.

References

[1] M.C. Flemings, Solidification processing, Metall. Trans. 5 (10) (1974) 2121–2134.
[2] T.M. Pollock, S. Tin, Nickel-based superalloys for advanced turbine engines: chemistry, microstructure and properties, J. Propul. Power 22 (2) (2006) 361–374.
[3] J. Campbell, Castings, Elsevier, 2003.
[4] D. Walton, U.B. Chalmers, The origin of the preferred orientation in the columnar zone of ingots, Trans. Am. Inst. Min. Metall. Eng. 215 (3) (1959) 447–457.
[5] M. Rappaz, C.-A. Gandin, Probabilistic modelling of microstructure formation in solidification processes, Acta Metall. Mater. 41 (2) (1993) 345–360.
[6] C.-A. Gandin, M. Rappaz, A coupled finite element-cellular automaton model for the prediction of dendritic grain structures in solidification processes, Acta Metall. Mater. 42 (7) (1994) 2233–2246.
[7] C.-A. Gandin, M. Rappaz, A 3d cellular automaton algorithm for the prediction of dendritic grain growth, Acta Mater. 45 (5) (1997) 2187–2195.
[8] M. Rappaz, C.A. Gandin, J.-L. Desbiolles, P. Thevoz, Prediction of grain structures in various solidification processes, Metall. Mater. Trans. A 27 (3) (1996) 695–705.
[9] Y. Zhou, A. Volek, N. Green, Mechanism of competitive grain growth in directional solidification of a nickel-base superalloy, Acta Mater. 56 (11) (2008) 2631–2637.
[10] H. Yu, J. Li, X. Lin, L. Wang, W. Huang, Anomalous overgrowth of converging dendrites during directional solidification, J. Cryst. Growth 402 (2014) 210–214.
[11] N. D’souza, M. Ardakani, A. Wagner, B. Shollock, M. McLean, Morphological aspects of competitive grain growth during directional solidification of a nickel-base superalloy, cmsx4, J. Mater. Sci. 37(3) (2002) 481–487.
[12] A. Wagner, B. Shollock, M. McLean, Grain structure development in directional solidification of nickel-base superalloys, Mater. Sci. Eng.: A 374 (1–2) (2004) 270–279.
[13] X. Meng, Q. Lu, X. Zhang, J. Li, Z. Chen, Y. Wang, Y. Zhou, T. Jin, X. Sun, Z. Hu, Mechanism of competitive growth during directional solidification of a nickel-base superalloy in a three-dimensional reference frame, Acta Mater. 60 (9) (2012) 3965–3975.
[14] A. Karma, W.-J. Rappel, Quantitative phase-field modeling of dendritic growth in two and three dimensions, Phys. Rev. E 57 (4) (1998) 4323.
[15] W.J. Boettinger, J.A. Warren, C. Beckermann, A. Karma, Phase-field simulation of solidification, Ann. Rev. Mater. Res. 32 (1) (2002) 163–194.
[16] D. Tourret, A. Karma, Growth competition of columnar dendritic grains: a phase-field study, Acta Mater. 82 (2015) 64–83.
[17] J. Li, Z. Wang, Y. Wang, J. Wang, Phase-field study of competitive dendritic growth of converging grains during directional solidification, Acta Mater. 60 (4) (2012) 1478–1493.
[18] T. Takaki, M. Ohno, Y. Shibuta, S. Sakane, T. Shimokawabe, T. Aoki, Two-dimensional phase-field study of competitive grain growth during directional solidification of polycrystalline binary alloy, J. Cryst. Growth 442 (2016) 14–24.
[19] A. Viardin, M. Založnik, Y. Souhar, M. Apel, H. Combeau, Mesoscopic modeling of spacing and grain selection in columnar dendritic solidification: envelope versus phase-field model, Acta Mater. 122 (2017) 386–399.
[20] T. Takaki, T. Shimokawabe, M. Ohno, A. Yamanaka, T. Aoki, Unexpected selection of growing dendrites by very-large-scale phase-field simulation, J. Cryst. Growth 382 (2013) 21–25.
[21] C. Beckermann, H.-J. Diepers, I. Steinbach, A. Karma, X. Tong, Modeling melt convection in phase-field simulations of solidification, J. Comput. Phys. 154 (2) (1999) 468–496.
[22] Y. Lu, C. Beckermann, J.C. Ramirez, Three-dimensional phase-field simulations of the effect of convection on free dendritic growth, J. Cryst. Growth 280 (1–2) (2005) 320–334, https://doi.org/10.1016/j.jcrysgro.2005.03.063.
[23] C. Wang, C. Beckermann, Equiaxed dendritic solidification with convection: Part i. multiscale/multiphase modeling, Metall. Mater. Trans. A 27 (9) (1996) 2754–2764.
[24] T. Okamoto, K. Kishitake, Dendritic structure in unidirectionally solidified aluminum, tin, and zinc base binary alloys, J. Cryst. Growth 29 (2) (1975) 137–146.
[25] A. Choudhury, B. Nestler, Grand-potential formulation for multicomponent phase transformations combined with thin-interface asymptotics of the double-obstacle potential, Phys. Rev. E 85 (2012) 021602, , https://doi.org/10.1103/PhysRevE.85.021602.
[26] J. Hötzer, M. Jainta, P. Steinmetz, B. Nestler, A. Dennstedt, A. Genau, M. Bauer, H. Köstler, U. Rüde, Large scale phase-field simulations of directional ternary eutectic solidification, Acta Mater. 93 (2015) 194–204.
[27] P. Steinmetz, Y.C. Yabansu, J. Hötzer, M. Jainta, B. Nestler, S.R. Kalidindi, Analytics for microstructure datasets produced by phase-field simulations, Acta Mater. 103

(2016) 192–203.
[28] V.P. Laxmipathy, F. Wang, M. Selzer, B. Nestler, K. Ankit, Influence of melt convection on the morphological evolution of seaweed structures: Insights from phase-field simulations, Comput. Mater. Sci. 170 (2019) 109196.
[29] B. Nestler, H. Garcke, B. Stinner, Multicomponent alloy solidification: Phase-field modeling and simulations, Phys. Rev. E 71 (2005) 041609, , https://doi.org/10.1103/PhysRevE.71.041609.
[30] N. Moelans, A quantitative and thermodynamically consistent phase-field interpolation function for multi-phase systems, Acta Mater. 59 (3) (2011) 1077–1086.
[31] A. Choudhury, M. Kellner, B. Nestler, A method for coupling the phase-field model based on a grand-potential formalism to thermodynamic databases, Curr. Opin. Solid State Mater. Sci. 19 (5) (2015) 287–300.
[32] A. Karma, Phase-field formulation for quantitative modeling of alloy solidification, Phys. Rev. Lett. 87 (2001) 115701, , https://doi.org/10.1103/PhysRevLett.87.115701.
[33] X. Tong, C. Beckermann, A. Karma, Q. Li, Phase-field simulations of dendritic crystal growth in a forced flow, Phy. Rev. E 63 (6) (2001) 061601.
[34] A. Vondrous, M. Selzer, J. Hötzer, B. Nestler, Parallel computing for phase-field models, Int. J. High Perform. Comput. Appl. 28 (1) (2014) 61–72.
[35] A. Zhang, S. Meng, Z. Guo, J. Du, Q. Wang, S. Xiong, Dendritic growth under natural and forced convection in al-cu alloys: From equiaxed to columnar dendrites and from 2d to 3d phase-field simulations, Metall. Mater. Trans. B 50 (3) (2019) 1514–1526.
[36] N. Shevchenko, O. Roshchupkina, O. Sokolova, S. Eckert, The effect of natural and forced melt convection on dendritic solidification in ga–in alloys, J. Cryst. Growth 417 (2015) 1–8.
[37] R. Kobayashi, Modeling and numerical simulations of dendritic crystal growth, Physica D 63 (3–4) (1993) 410–423.